Hindawi
Advances in Civil Engineering
Volume 2019, Article ID 9504101, 14 pages
https://doi.org/10.1155/2019/9504101

Research Article

A Study of Fractal Deep-Hole Blasting and Its Induced Stress Behavior of Hard Roof Strata in Bayangaole Coal Mine, China

Jianping Zuo,[1,2] **Zhengdai Li**,[1] **Shankun Zhao**,[3] **Yunqian Jiang**,[1] **Haiyan Liu**,[1] **and Maohong Yao**[1]

[1]*School of Mechanics and Civil Engineering, China University of Mining and Technology, Beijing 100083, China*
[2]*State Key Laboratory of Coal Resources and Safe Mining, China University of Mining and Technology, Beijing 100083, China*
[3]*Mine Safety Technology Branch, China Coal Research Institute, Beijing 100013, China*

Correspondence should be addressed to Jianping Zuo; zjp@cumtb.edu.cn

Received 7 May 2018; Revised 19 December 2018; Accepted 3 January 2019; Published 3 February 2019

Academic Editor: Daniele Baraldi

The phenomena of strong pressure occurrences have been observed many times in the #311103 working face of the Bayangaole Coal Mine. Deep-hole blasting measures were used to relieve the pressure in order to decrease the danger levels of these strong pressure occurrences on the working face. The blasting layouts proposed in this study differed from the conventional blasting layouts of a "straight-line" design by instead utilizing "triangular-fractal" and "deep-shallow-fractal" for the purpose of successfully driving the explosive efficiency and enlarging the roof-blasting range. The fractal dimension of the "triangular-fractal" blasting layout was calculated as 1.1274. The fractal dimension of the "deep-shallow-fractal" was calculated to be 1.556. The fractal dimensions of both improved layouts were found to be larger than that of the "straight-line" blasting layout (1.0). In addition, the Mises stress evolution and the changed trend of the effective stress and strain of the observation points around the hole of the three layouts are analyzed and compared by LS-DYNA numerical simulation software. The results indicated that the "deep-shallow-fractal" blasting layout had the most effective blasting effects, followed by the "triangular-fractal" blasting layout. It was determined that the traditional "straight-linear" blasting layout had the least effective blasting effects of the three examined layouts. In summary, the implementations of the improved fractal blasting layouts in this study were found to be conducive to the enhancement of the blasting effects.

1. Introduction

With the progress of the working face in the Bayangaole Coal Mine, the hard roof is suspended in the goaf area. Due to the large strength and thickness of the mine's roof, a large area pressure phenomenon had occurred on the working face [1, 2] which brought serious hidden hazards to the mine production processes [3, 4]. Therefore, it was necessary to take effective measures for roof weakening in order to prevent potential accidents in the mine. At the present time, the most widely used roof-weakening techniques mainly involve hydraulic and blast-fracturing technology [5–9]. Blast-fracturing technology is used to expand the crack zones, thereby destroying the integrity of the rock masses. This results in causing the roof areas to fall more easily.

Many research studies and explorations regarding coal and rock blasting in coal mines have been conducted in China and internationally. Paine and Please [10] studied the destructive mechanical effects of the detonation gas on cracks in hard roof of coal mine and proposed an improved model of fracture propagation by gas during rock blasting; Xie et al. [11–13] used the fractal theory to establish the theoretical relationship between the dissipative energy of fractured rock in hard roof and the fractal dimension value of the block; Song and Kim [14] studied the entire process of rock damage by numerical simulation and described the initiation and propagation of cracks through different mechanisms and processes; and Trivino and Mohanty [15] have assessed single-hole blast-induced damage in a granitic outcrop through both numerical simulations with a combined

finite-discrete element method (FEM-DEM) and controlled experiments. Lu and Tao [16] theoretically examined the velocities of the crack propagations driven by the detonation gases. Zuo et al. [17] carried out fracture mechanics analyses of the first roof falling presplitting blasting mechanisms of working faces. Banadaki and Mohanty [18] studied the damage of stress wave to roof rock through numerical simulation.

At present, the roof blasting of the coal mine working face has made a lot of progress, but due to the complex geological environment of deep rock mass, the roof of different coal mine working faces has different properties, so the traditional roof blasting method cannot fully adapt to all kinds of roof blasting. The phenomenon of strong pressure has been found to have occurred 27 times in the #311103 working face of the Bayangaole Coal Mine. In order to reduce the risks of these strong pressure occurrences in the working face of the mine and improve the blasting effects of blast holes during the mining process, the mechanism of deep-hole blasting in thick and hard coal mine roof was studied. Then, the blasting behaviors of the different blasting layouts were optimized and analyzed based on the fractal theory presented in this study. The blasting process was simulated using LS-DYNA numerical simulation software in order to discuss the stress and strain evolution laws of the different blasting layouts. The goal was to obtain the optimal blasting layout and provide theoretical guidance for similar thick and hard-roofed mining conditions during presplitting blasting processes.

2. Engineering Conditions

The Bayangaole Coalfield is located in the southern section of the Hugierte exploration area, approximately 30 km west of the town Dabuchake in Wushen County. There are 10 layers of coal deposits currently being mined in the coalfield, of which the 3–1 and 5–1 coal seams are minable within the entire area. The 3–1 coal seam has been determined to be stable. This seam has a thickness ranging from 3.09 to 7.00 m, with an average thickness of 5.74 m. The thickness increases gradually from north to south. The roof of the haulage roadway, and the return airway of the #311103 working face, was determined to be comprised of sandy mudstone measuring approximately 12.2 m; medium-grain sandstone measuring approximately 12.96 m; fine sandstone measuring approximately 3.74 m; and medium-grain sandstone measuring approximately 13.45 m, respectively. The stratigraphic structure of the areas is shown in Figure 1.

According to the blasting data provided by the Bayangaole Coal Mine, in the #311103 working face, strong pressure phenomena have been occurred 27 times, and the specific situations of "strong pressure phenomena" are listed in Table 1. It contains the location and date of the occurrence and the distance from the last strong pressure phenomenon.

The phenomenon of strong pressure which had occurred within 50 m ahead of the #311103 working face was violent. Therefore, blasting pressure relief measures were recommended to be utilized in the subsequent relevant areas in order to reduce the risks of strong pressure conditions on the working face of the mine.

In deep-hole blasting, there is a need to blast the key stratas. According to the key strata theory [19], the key strata of the 311103 working face roof rock layer is calculated by the following formula:

$$(q_n)_1 = \frac{E_1 h_1^3 (\gamma_1 h_1 + \gamma_2 h_2 + \ldots + \gamma_n h_n)}{E_1 h_1^3 + E_2 h_2^3 + \ldots + E_n h_n^3}. \quad (1)$$

Introducing the parameters of the roof rock layer into formula (1), the results are presented in Table 2. The two layers of the medium-grain sandstone above the #311103 working surface are calculated to be the key strata. Therefore, the second layer of the medium-grain sandstone needs to be blasted in the deep-hole blasting process. Considering the difficulties in practical construction, the 45° drilling angle is the easiest to implement, and the corresponding drilling depth is calculated to be about 45 m.

At the present time, blast-caving processes are often used to relieve pressure in hard and thick roof areas. However, long cantilever roofs will be formed behind the working face if caving is not in place, which potentially results in major hidden dangers for production and construction processes. Consequently, it is necessary to analyze the blasting mechanisms of the roof rock in mines, as well as predict the influence scope of the rock fragmentations, in order to determine the most effective blasting layout for the explosion of key strata in sandstone layers.

In order to calculate the theoretical blasthole spacing and the mechanical parameters of the medium-grain sandstone used in the simulation, it is necessary to conduct laboratory tests on the grain sandstone in the key layer of the roof.

In this research study, uniaxial compression and Brazilian splitting tests were carried out on the sandstone of the roof-blasting strata of the #311103 working face using a GCTS servohydraulic machine obtained from the laboratory of the China University of Mining and Technology (Beijing), as detailed in Figures 2–4.

The uniaxial compressive strength was obtained by taking the average value of the three specimens obtained with the GCTS. The tensile strength of the rock was indirectly obtained by the Brazilian splitting test method. The peak load of the three specimens was then converted into the maximum tensile stress of the specimen according to formula (2). The tensile strength of the sandstone was obtained by taking the mean value. The peak loads of the three specimens in the Brazilian splitting test were separately substituted into formula (2) in order to determine the maximum tensile stress of the rock. Then, the tensile strength of the sandstone could be calculated by the mean value [20] as follows:

$$\sigma_t = \frac{2P}{\pi d t}, \quad (2)$$

where σ_t represents the maximum tensile stress at the center of the specimen; P denotes the extreme pressure of the specimen's failure; d is the specimen's diameter; and t is the thickness of the specimen. The physical and mechanical parameters of the sandstone are shown in Table 3.

Column shape	Rock types	Thickness (m)	Lithological description
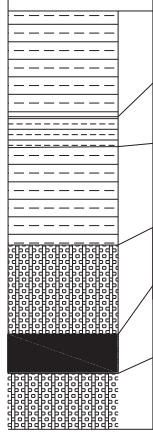	Medium grain sandstone	13.45	Pale grayish white, mainly quartz, with cuttings and mica
	Fine grain sandstone	3.74	Pale, wavy bedding, with cuttings and mica
	Medium grain sandstone	12.96	Pale grayish white, mainly quartz, with cuttings and mica
	Sandy mudstone	12.2	Dark gray, uniform with sand, flat fracture
	3-1 coal	5.74	Black, dark coal containing silk carbon
	Sandy mudstone	6.75	Dark gray, uniform with sand, flat fracture

Figure 1: Integrated strata histogram.

Table 1: #311103 working face strong pressure phenomena statistical table.

Number	Date	Mining distance (m)	Distance from the last strong pressure (m)
1	2017.04.28	210.3	
2	2017.06.01	453.4	243.1
3	2017.06.04	474.2	20.8
4	2017.06.22	558.4	84.2
5	2017.06.26	601.2	42.8
6	2017.06.29	634.5	33.3
7	2017.07.01	654.9	20.4
8	2017.07.04	698.7	43.8
9	2017.07.12	756.1	57.4
10	2017.07.23	828.3	72.2
11	2017.07.29	876.2	47.9
12	2017.08.03	908.8	32.6
13	2017.08.10	964.2	55.4
14	2017.08.23	1045.7	81.5
15	2017.08.29	1134.0	88.3
16	2017.09.02	1154.4	20.4
17	2017.09.17	1331.3	176.9
18	2017.09.30	1444.6	113.3
19	2017.10.06	1513.9	69.3
20	2017.10.08	1533.4	19.5
21	2017.10.18	1589.1	55.7
22	2017.10.28	1736.5	147.4
23	2017.10.30	1771.1	34.6
24	2017.11.15	1955.4	184.3
25	2017.11.19	1998.6	43.2
26	2017.11.21	2010.6	12.0
27	2017.11.28	2088.4	77.8

Table 2: #311103 working face key strata calculation statistics table.

Type of rock	Thickness of each layer h_i (m)	Volume force γ_i (kN/m^3)	Elastic modulus E_i (GPa)	$(q_n)_1$	Calculated result
Medium-grain sandstone	13.45	23	23	326.16	The key strata
Fine grain sandstone	3.5	24	21	380.69	—
Medium-grain sandstone	12.96	23	23	298.08	The key strata
Sandy mudstone	12.2	25	15		—

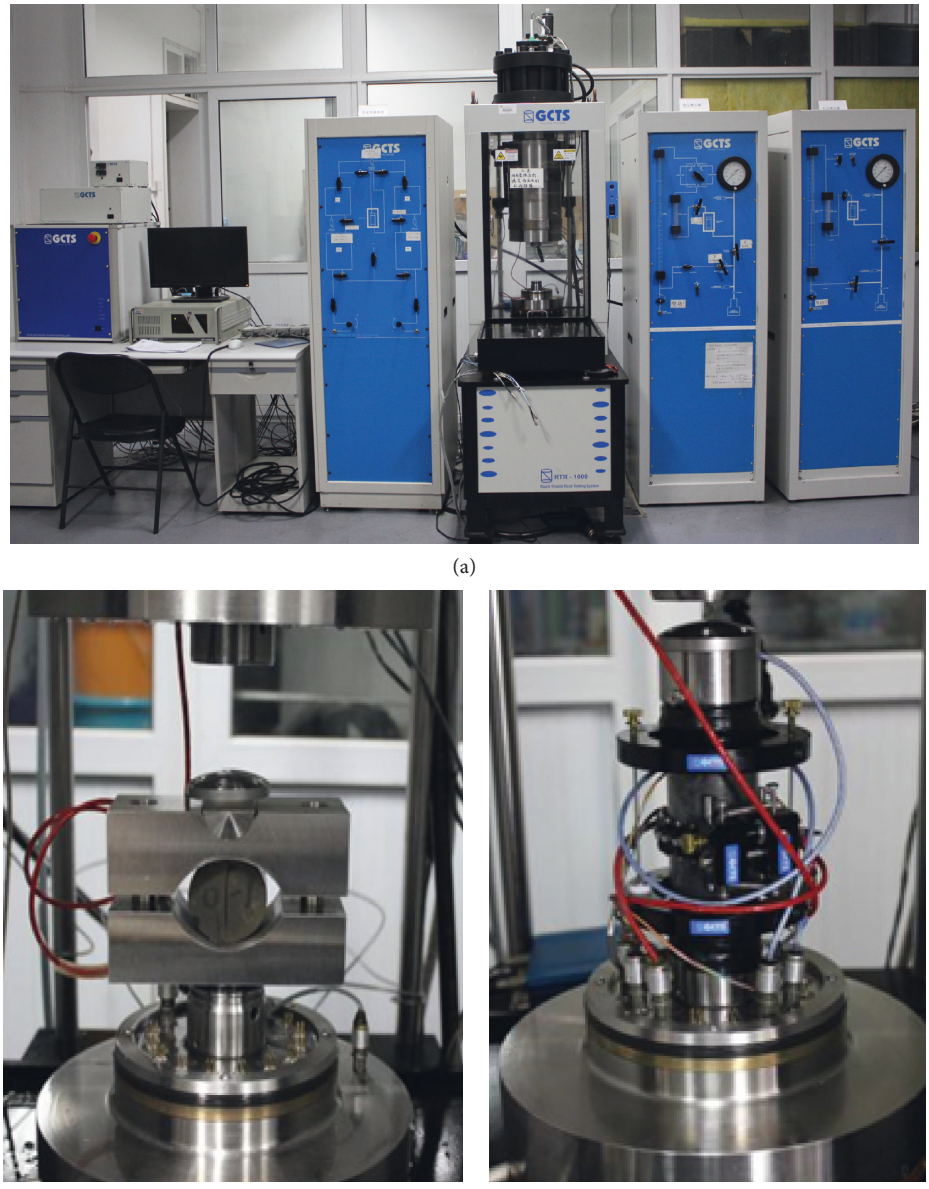

(a)

(b) (c)

Figure 2: Compression and tensile experiments of sandstone. (a) GCTS servohydraulic machine. (b) Brazilian splitting test. (c) Uniaxial compression test.

3. Analyses of the Crushing Mechanism and Scope of Deep-Hole Blasting in Hard Roof

3.1. Analysis of the Crushing Mechanism of the Deep-Hole Blasting in Hard Roof. The effects of explosives on rock fragmentation mainly include the compression and tension processes of the blasting stress waves and the expansion processes following the detonation gases entering the rock cracks. For deep-hole blasting, the free surfaces of the roof areas cannot play the roles of reflection and stretching. As a result, the stress waves become reverberated and stretched by the joint surfaces and microcracks inside the rock masses. In this study, the damages caused to the rock due to stress waves are shown in Figure 5. Under the initial compression and tension of the stress waves, the preexisting fractures in the rock formed the initial cracks. The detonation gases entered into the initial cracks, which then exerted vertical stresses resulting in further crack propagation. When the stress intensity factor K_I at the crack tips reached the critical value of the rock fracture toughness K_{IC}, the crack performed an "opening mode" propagation [21]. K_I could then be expressed as follows [22]:

$$K_I = QP_c\sqrt{\pi a}, \tag{3}$$

where P_c is the quasi-static pressure of the explosive gases acting on the rock wall; a is the crack length in the rock mass; and Q denotes the stress intensity factor correction factor, which increased as the crack length a increased. It can be

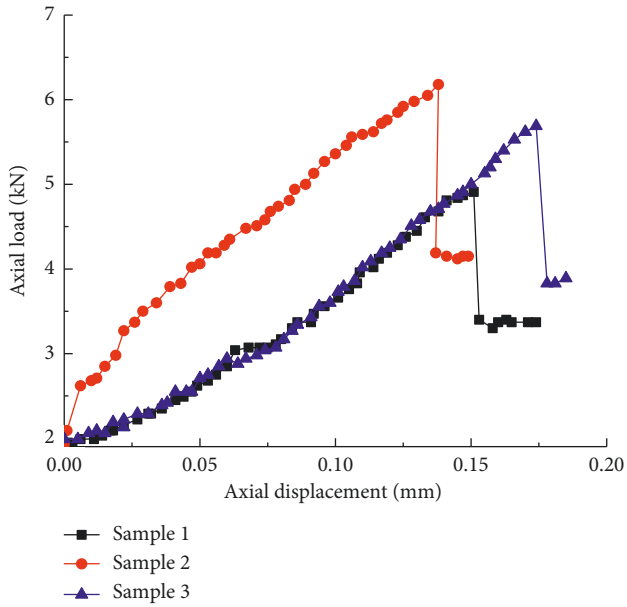

Figure 3: Brazilian split test curve.

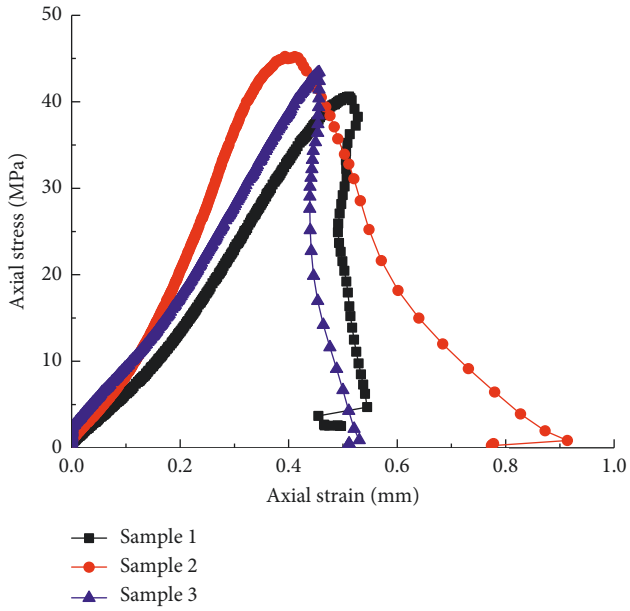

Figure 4: Uniaxial compressive strength curve.

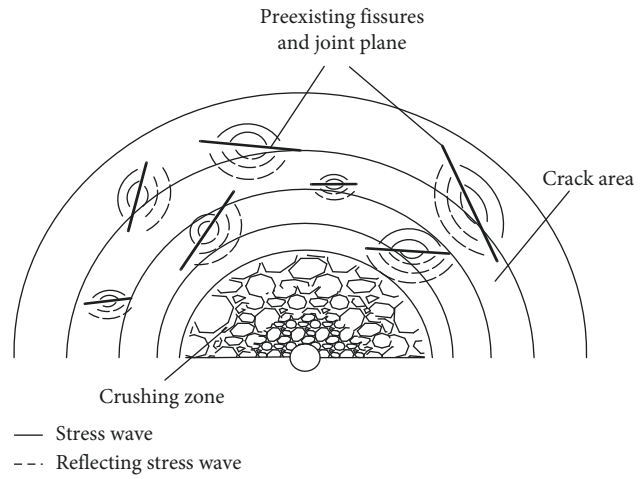

Figure 5: The effect of stress wave on rocks.

Table 3: Physical and mechanical parameters of sandstone.

Density ($kg \cdot m^{-3}$)	Uniaxial compressive strength (MPa)	Uniaxial tensile strength (MPa)	Poisson's ratio
2130.8	43.94	2.8515	0.2225

seen in formula (3) that, with the elongations of the fracture lengths, greater explosive gas pressure was generated and resulted in more opportunities for the propagation and extension of the fractures.

The energy which had been produced by the explosion gradually dissipated in the form of stress waves and detonation gases. The results of related studies have indicated that the fractures in the rock masses occurred when the instantaneous energy density on the fracture surface reached a critical value [23], and the critical energy density could then be calculated as follows:

$$E_{cr} = \frac{C_p}{E} \int_0^{\tau} \sigma^2 dt, \tag{4}$$

where σ denotes the stress waves acting on the rock mass; τ is the action time of the stress waves; C_p is the wave velocity of the rock; and E represents the elastic modulus of the rock. As the action time, energy density, and intensity of the stress wave increased, the inclination of rock failure was more easily germinated.

From the perspective of fractures and energy, it was determined that improving the length and number of

cracks in the fracture area at the initial stage of blasting, along with simultaneously slowing down the diffusion rate and attenuation of the stress waves, was beneficial to enhancing the blasting effects.

3.2. Analysis of the Influence Scope of the Deep-Hole Blasting in Hard Roof. The deep-hole blasting of the roof was required to produce an increased number of cracks around the blast holes. These cracks needed to penetrate between the adjacent blast holes in order to weaken the roof areas. Then, by simultaneously considering the efficiency of the construction and economic factors, the crack zones generated by the adjacent blast holes were required to be in tangent with each other. The expressions of the blastholes intervals obtained from the Mises criterion were as follows [24]:

$$d = 2r_b\left(\frac{\sqrt{2}\,\sigma_R B}{2\sigma_{td}}\right)^{1/\beta}\left(\frac{\sqrt{2}\,\rho_0 D^2 n k^{-2\gamma} l_e B}{16\sigma_{cd}}\right)^{1/\alpha}, \quad (5)$$

$$\begin{cases} \alpha = \dfrac{2-\mu_d}{1-\mu_d}, \\ \beta = \dfrac{2-3\mu_d}{1-\mu_d}, \\ b = \dfrac{u_d}{1-u_d}, \\ B = \sqrt{(1+b^2)+(1+b)^2-2\mu_d(1-\mu_d)(1-b)^2}, \end{cases} \quad (6)$$

where d denotes the blasthole intervals, m; σ_R is the radial stress on the interface between the crushing zone and the crack zone, $\sigma_R = \sqrt{2\sigma_{cd}/B}$; ρ_0 and ρ represent the density of the explosives and rock mass, respectively, kg/m^3; D is the explosive velocity, m/s; C_p denotes the longitudinal wave velocity, m/s; σ_{cd} is the dynamic tensile strength of rock, MPa; α represents the load transmission attenuation index; β is the stress wave attenuation index; σ_{td} is the dynamic uniaxial tensile strength of rock, MPa; b is the lateral stress coefficient; μ_d denotes the rock dynamic Poisson's ratio, $\mu_d = 0.8\,\mu$; r_b represents the radius of the blast hole; B denotes the property parameters of the explosives; K represents the decoupling coefficient; γ is the adiabatic coefficient of the detonation products, which was generally set to 3; l_e represents the charge axial coefficient; and n is the increment coefficient of the expanding detonation product colliding with the hole wall, which was generally set to 10.

According to the data of the Bayangaole Mine's working face, the density of the medium-grain sandstone was 2,130.8 kg/m^3; C_p was set to 3,300 m/s in the rock stratum; μ_d was set to 0.178; and b was set to 0.126. The dynamic tensile strength of blasting σ_{td} changed slightly with the loading strain rate, and $\sigma_{td} = \sigma_t$ was set to 2.852 MPa. The dynamic compressive strength of the blasting σ_{cd} varied with the loading strain rate, where $\sigma_{cd} = 1.8$ and $\sigma_c = 79.1$ MPa in this research study. Also, $K = 1.3$ adopted a continuous charge with $l_e = 1$. The parameter values were substituted into formula (5), and the crack zones were tangent with each other when the blasthole interval was 10.055 m.

4. Fractal Layout of the Deep-Hole Blasting in Hard Roof

4.1. Theoretical Analysis of the Fractal Blasting Layout of Hard Roof. During the process of the deep-hole blasting in the roof area, the fracture produced after the blasting was a fractal structure which had been formed by the fractal behavior of the evolution and agglomeration of the microcracks and joints. The relationship between the fractal dimension and the energy distribution and dissipation was determined to be as follows [17]:

$$D_f = a + b\lg E, \quad (7)$$

where $a = \lg E/\lg r$; $b = 3 - \lg C/\lg r$; C represents a material related constant; and r is the blasthole interval.

By using formula (7), it was determined that the value of the fractal dimension was proportional to the dissipative energy density. Then, with the increasing of the crack fractal dimensions following the blasting process, it was observed that the cracks which had been generated in the rock mass became more complex. The energy released from the explosion could be fully utilized, which led to more efficient blasting effects.

The fractal dimension of the self-similarity curve D_f could be expressed as follows [25]:

$$D_f = \frac{\lg N}{\lg(l/r)}, \quad (8)$$

where N is the number of line segments with equal lengths in a fractal geometry and l/r is the similarity ratio, which refers to the ratio of the distance between the two ends of a geometric figure to the total length of these line segments.

The fractal dimension characterized the irregular degree of the graph. As the fractal dimension D_f increased, the formations of the cracks became more complex and developed fissures more easily. During the process of the blasting, the coal mine roof became weakened, which improved the fractal dimensions of the blast holes, and more cracks were generated after explosions. These actions promoted the utilization rate of the blasting energy and attained the desired blasting results.

4.2. Calculation of the Fractal Dimensions in Three Blasting Layouts

4.2.1. "Straight-Line" Blasting Layout of the Roof Areas (Original Layout). In this layout, the blast holes were lined up in a straight line on the roof and were drilled into the rock above the coal seam at an elevation angle of 45 degrees. The lengths of the blast hole were 45 m, and the blast hole intervals were 10 m. The explosive loading position is shown in Figure 6. The length of the drug column was set at 8 m.

Since fractal geometry has self-similarity, l/r is the similarity ratio. In the "straight-line" blasting layout, three adjacent blast holes were regarded as a group of fractal graphics (Figure 7).

In the "straight-line" blasting layout, as well as the two fractal blasting layouts discussed later, three adjacent blast

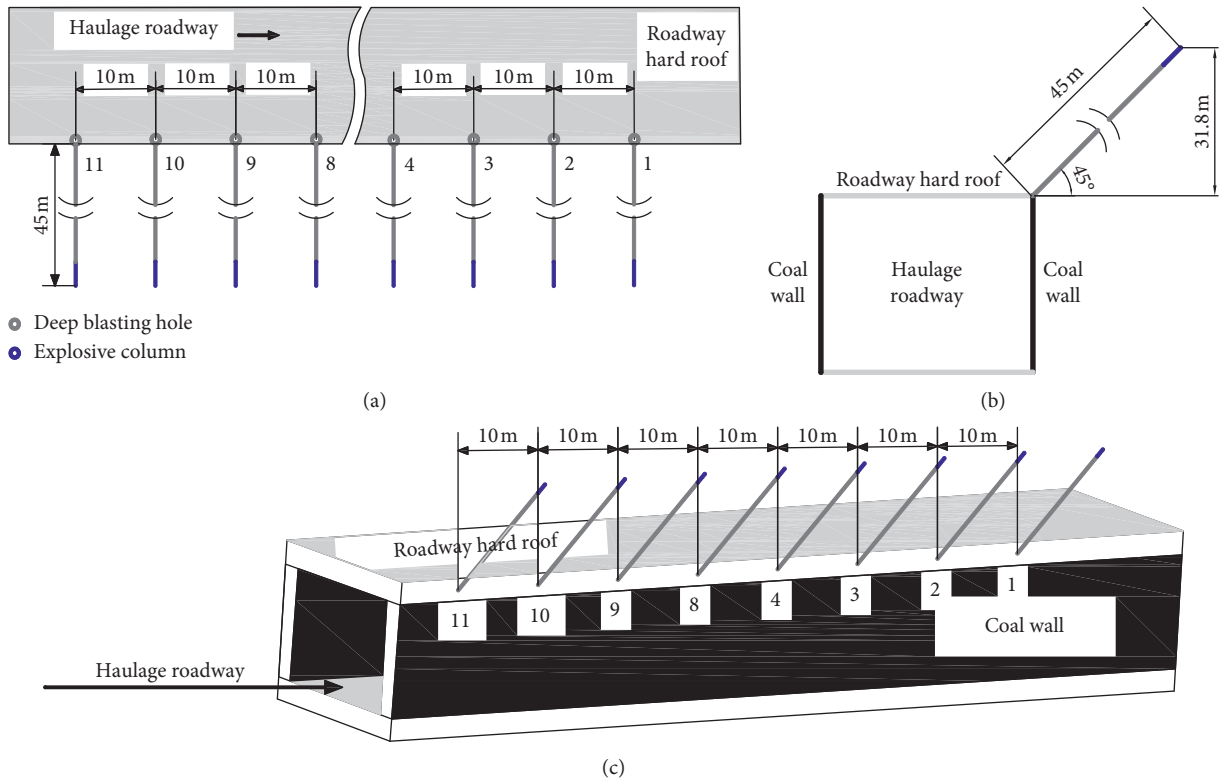

Figure 6: "Straight-line" blasting layout. (a) Top view of blasting layout. (b) Cross-sectional view of blasting layout. (c) 3D drilling position.

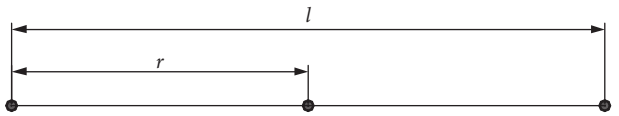

Figure 7: Fractal graphics of "straight-line" blasting layout.

holes were regarded as a group of fractal graphics. The relevant parameters were obtained as follows: $l = 20$ m, $r = 10$ m, $l/r = 2$, and $N = 2$. Then, the fractal dimension of the "straight-line" blasting layout was $D_f = 1.0$.

4.2.2. "Triangular-Fractal" Blasting Layout of the Roof (Optimization Layout 1). The blast holes in this layout were arranged in a double row dislocation (triangle) on the roof and had the same drilling lengths and angles as the "straight-line" blasting layout (Figure 8). It was considered that the blasthole position should be close to the angle of the wall and roof of the coal mine and reveal the fractal characteristics of the layout. Moreover, the row spacing was set at 2 m, and the blasthole intervals were set at 10 m. The length of the drug column was set to 8 m as in the straight-line layout.

In the "triangular-fractal" blasting layout, three adjacent blast holes were considered to be a group of fractal graphics (Figure 9).

The relevant parameters were gained as follows: $N = 2$, row spacing $d = 2$ m. The length of the line segment $r = \sqrt{10^2 + d^2} = 10.198$ m, $l/r = 1.9394$, and then, the fractal dimension of the "triangular-fractal" blasting layout $D_f = 1.1274$.

4.2.3. "Deep-Shallow-Fractal" Blasting Layout (Optimization Layout 2). In this optimized layout, the blast holes were located in a straight line and drilled into the rock above the coal pillar at an elevation angle of 45 degrees, with the same angle as the "straight-line" blasting layout (Figure 10). The drilling lengths were alternately set as 45 m for the deep hole and 37 m for the shallow hole, with blasthole intervals of 10 m. The length of the drug column was set as 8 m.

In the "deep-shallow-fractal" blasting layout, three adjacent blast holes were defined as a group of fractal graphics (Figure 11).

In the "deep-shallow-fractal" blasting layout, $N = 2$ and $r = 10$ m were given, and the lengths of shallow and deep blast holes were 37 m and 45 m, respectively. Since the length of the drug column was 8 m, the midpoints of each drug column were taken as the calculating points. Then, $N = 2$, $d = 8$ m, $r = \sqrt{10^2 + d^2} = 12.81$ m, and $l/r = 1.5613$ were derived. The fractal dimension of the "deep-shallow-fractal" blasting layout is $D_f = 1.556$.

The blasting layouts with larger fractal dimensions produced more cracks and thereby improved the blasting effects. The fractal dimensions of the three blasting layouts are shown in Table 4.

5. Simulation Analysis of the Deep-Hole Optimized Blasting Layouts for Hard Roof

In order to select the most effective blasting layout, the processes of the three blasting layouts were simulated using LS-DYNA. The Mises stress nephogram, an equivalent stress

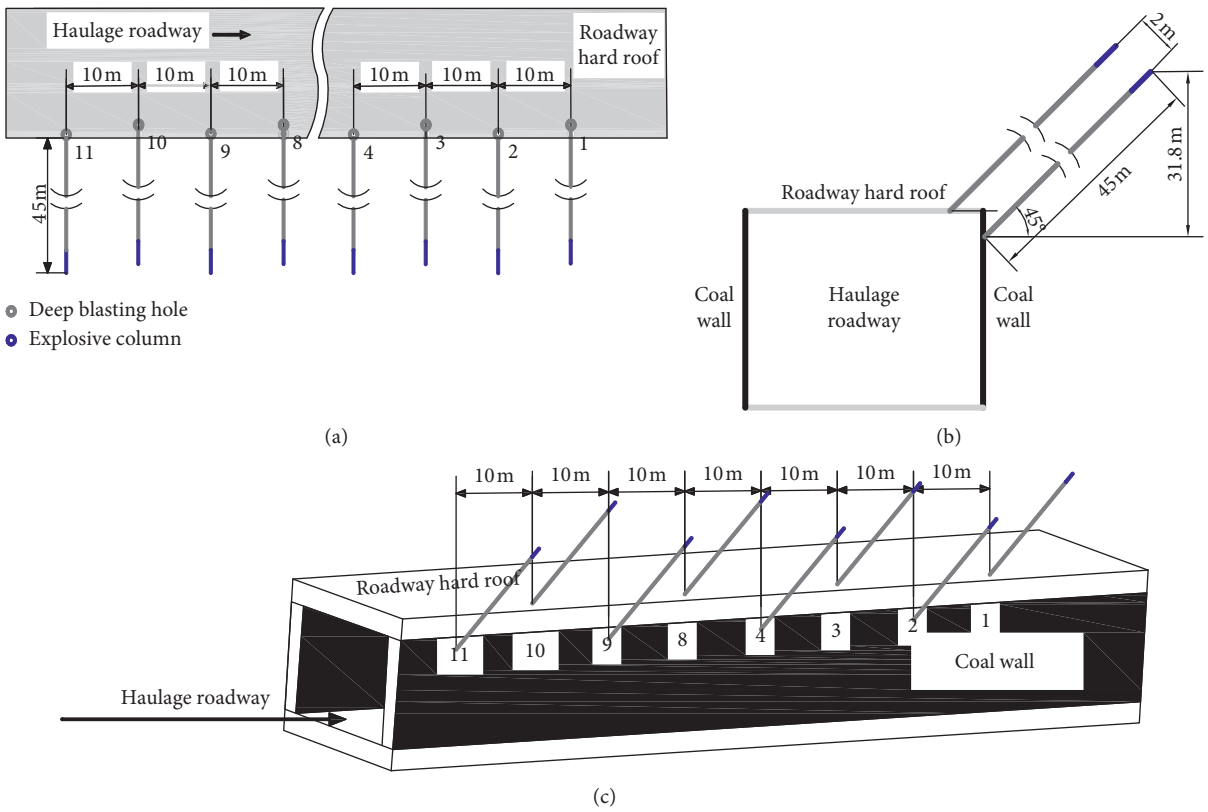

Figure 8: "Triangular-fractal" blasting layout. (a) Top view of blasting layout. (b) Cross-sectional view of blasting layout. (c) 3D drilling position.

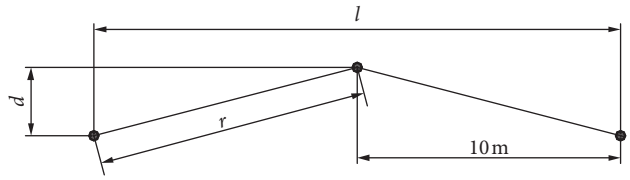

Figure 9: Fractal graphics of "triangular-fractal" blasting layout.

map of the observation points, and the strain maps obtained from the simulation were analyzed, and a comparison was made.

5.1. Blasting Simulation Constitutive Model. In Part 2, deep-hole blasting is believed to be conducted at the key strata. Two layers of the medium-grain sandstone are calculated as key strata. In order to effectively relieve the pressure on the top roof, the blasthole needs to be driven into the second layer of the key strata for blasting. The purpose of this simulation is mainly to study the influence of different blasting layouts on the blasting effects of the key layer, so only the key strata rock is simulated. The relevant parameters of the medium-grain sandstone applied in the simulation are listed in Table 5.

A coupling charge structure was used in this study's simulation process, and a JWL constitutive equation [26] was applied to express the explosion effects, as shown in the following equation:

$$P = A\left(1 - \frac{\omega}{R_1 V}\right)e^{-R_1 V} + B\left(1 - \frac{\omega}{R_2 V}\right)e^{-R_2 V} + \frac{\omega E_0}{V}, \quad (9)$$

where A and B are the explosive parameters, GPa; R_1, R_2, and ω are the explosive parameters; P is the pressure, MPa; E_0 denotes the internal energy of the detonation product; and V is the relative volume of the detonation product, m^3. The values of the specific parameters (s) are listed in Table 6.

In addition to the relevant blasting parameters in Table 6, the property of the explosive itself has a significant impact on blasting. The simulated explosive has a density of 1.3 g/cm^3, a detonation speed of 4000 m/s, and a detonation pressure PCJ of 9.9 GPa.

5.2. Selection of Monitoring Points in the Numerical Model. In view of the actual length of the roadway, large number of holes, and processing capacity of computer, this study selected three adjacent holes as the research simulation objects. The size of the model was 80 m × 80 m × 30 m.

Three observation points were utilized in each of the blasting layouts in order to monitor the processes of the stress and strain variations during the explosion. Figure 12 shows the positions of the monitoring points for the "straight-line," "triangular-fractal," and "deep-shallow-fractal" blasting layouts.

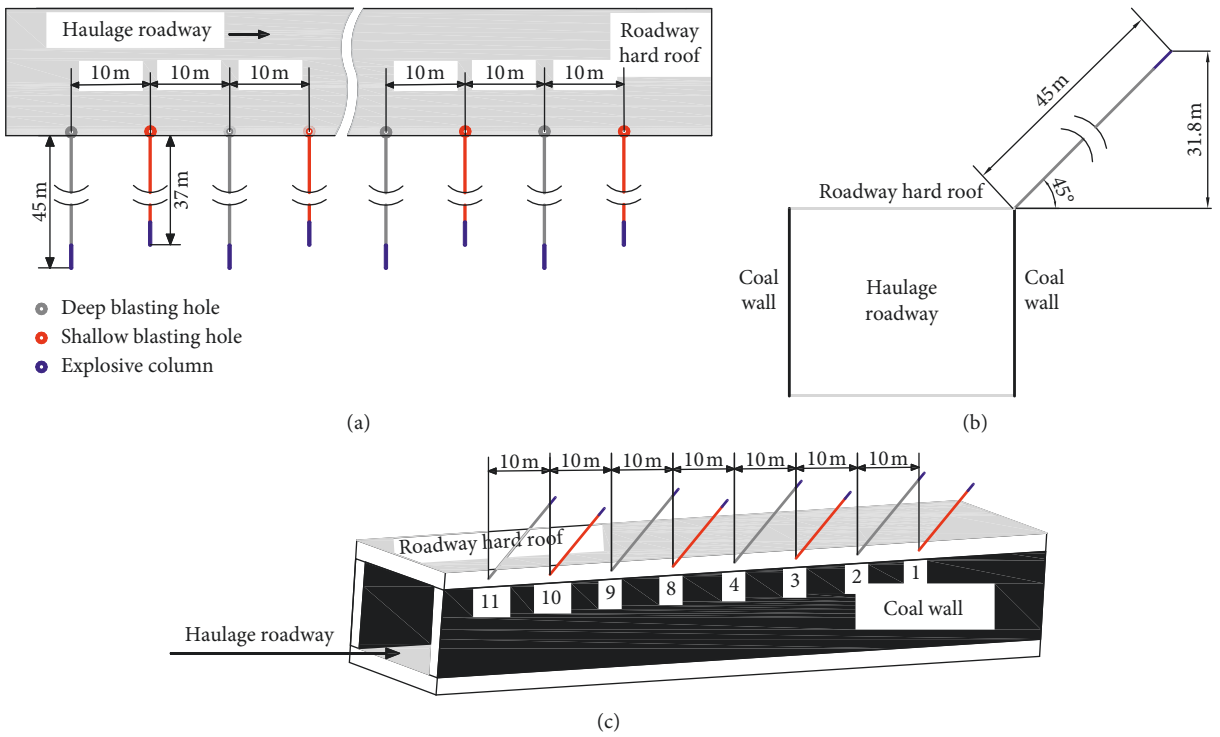

Figure 10: "Deep-shallow-fractal" blasting layout. (a) Top view of blasting layout. (b) Cross-sectional view of blasting layout. (c) 3D drilling position.

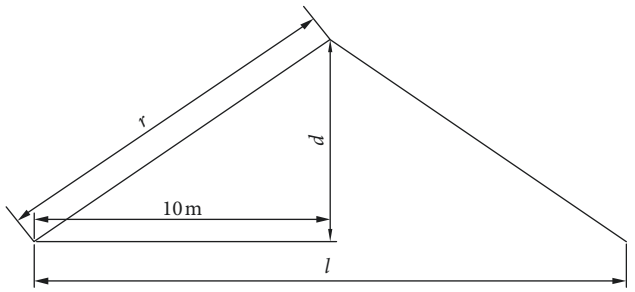

Figure 11: Fractal graphics of "deep-shallow-fractal" blasting layout.

Table 4: Fractal dimensions of the different blasting layouts.

Blasting layout	"Straight-line"	"Triangular-fractal"	"Deep-shallow-fractal"
Fractal dimension	1	1.1274	1.556

5.3. Analysis of the Numerical Simulation of Blasting Process

5.3.1. Simulation Analysis of the Stress. In numerical blasting simulations, the Mises stress is generally used to describe the complex stress variations during rock blasting and to characterize the blasting effects on the rock. The blasting effects can be measured by analyzing the stress scope in the Mises stress nephogram, as well as the Mises stress density in the blasting area and the decay rate of the stress wave. The processes of the Mises stress evolution of the three blasting layouts are shown in Figures 13–15.

As can be seen in Figures 13–15, the Mises stress range of the three schemes became reduced with the changes in the blasting times, and the strength of the stress had also gradually decreased. This was due to the fact that the energy generated by the explosive which was used in the three blasting layouts had destructive effects on the rock mass. This led to rock fractures or the formation of cracks which then consumed most of the energy. At that point, the weaker stress waves were gradually transmitted to the far ends, resulting in the energy from the blasting to be further dissipated.

The analysis results demonstrate that the stress concentration area (warm tone area) range and amplitude of the "deep-shallow-fractal" blasting layout were the largest. Also, the stress wave decay rate in the deep-shallow-fractal layout was observed to be the slowest, followed by that of the "triangle-fractal" blasting layout. Meanwhile, the "straight-line" blasting layout scheme displayed the smallest stress concentration area and amplitude, along with the fastest decay rate of the stress wave. It was concluded from the perspective of the Mises stress that the larger the fractal dimension of the blasting layout scheme, the slower the decay rate of the blasting energy. Therefore, it was determined that the process was able to make full use of the energy applied to the rock, which was conducive to the expectations of the formation and expansion of cracks in the rock mass.

Figure 16 shows the variations of the equivalent stress over time for the three monitoring points. In this study, by

Table 5: Medium-grain sandstone blasting parameters.

Mass density ($g \cdot cm^{-3}$)	Elastic modulus (GPa)	Maximum compressive strength (GPa)	Maximum tensile pressure (MPa)	Poisson's ratio	Accumulated plastic strain before fracture (%)
2.131	23	43.94	2.8515	0.2225	0.7

Table 6: Blasting parameters.

D ($m \cdot s^{-1}$)	A (GPa)	B (GPa)	R_1	R_2	ω	E_0 (GPa)
3600	214.4	0.182	4.2	0.9	0.15	4.19

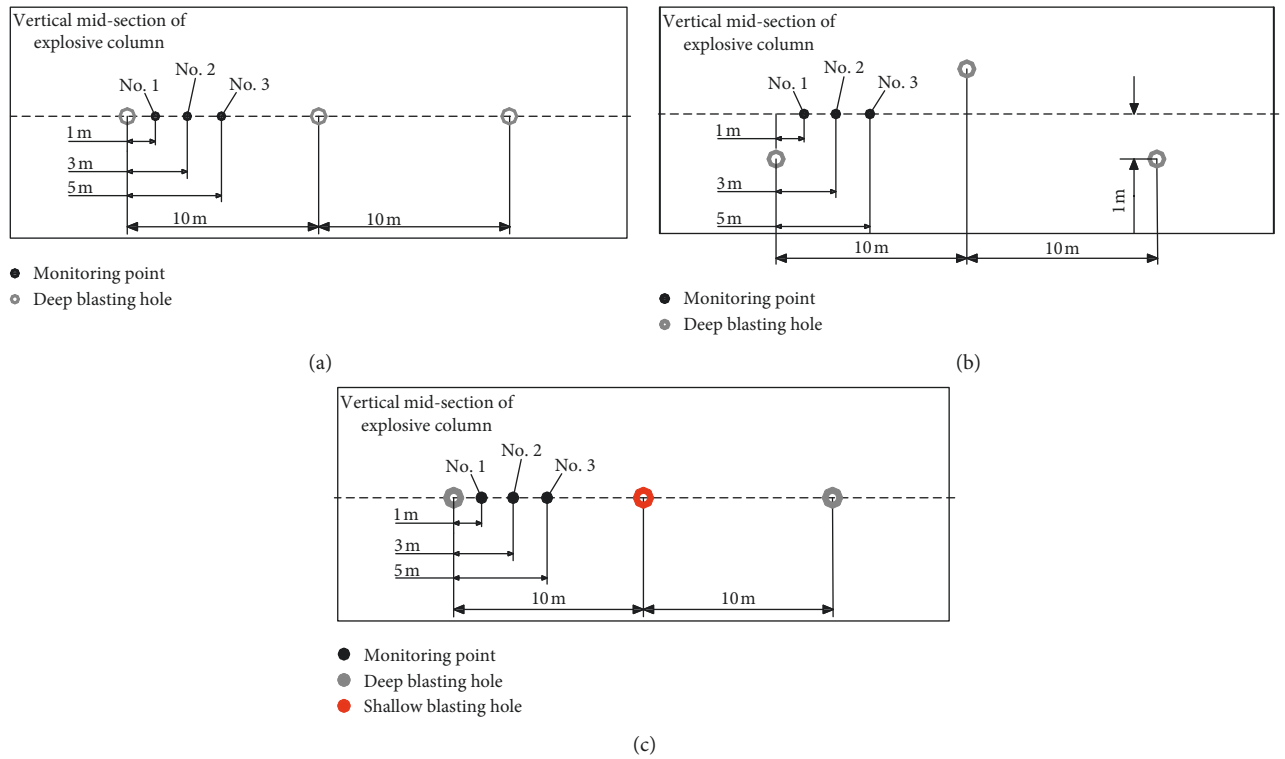

Figure 12: Location of monitoring points. (a) "Straight-line" blasting layout monitoring point location. (b) "Triangle-fractal" blasting layout monitoring point location. (c) "Deep-shallow-fractal" blasting layout monitoring point location.

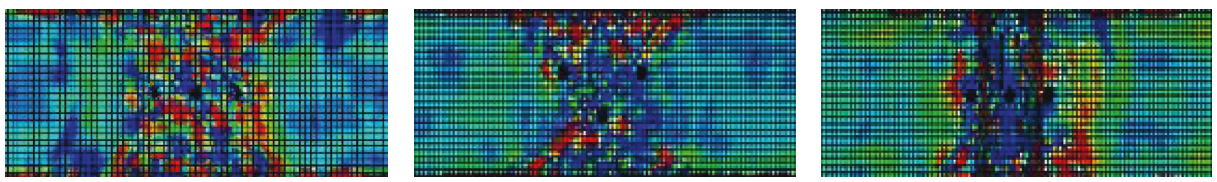

Figure 13: Mises stress nephogram of roof section in the next 0.15 ms after blasting. (a) "Straight-line" blasting layout. (b) "Triangle-fractal" blasting layout. (c) "Deep-shallow-fractal" blasting layout.

comparing the peak values of the equivalent stress at the monitoring points and the speed of the decay rate, the resulting damages at the different positions in the blasting area could be accurately judged.

Figure 16 displays the equivalent stress variation trends of the three monitoring points. Following the explosion, the equivalent stress of the monitoring points rapidly increased to the peak value. Then, the equivalent stress rapidly decreased and continuously oscillated. With the action of the blasting, the equivalent stress of the monitoring points gradually decreased and finally reached a zero value. Graphs (a), (b), and (c) represent the three monitoring points with

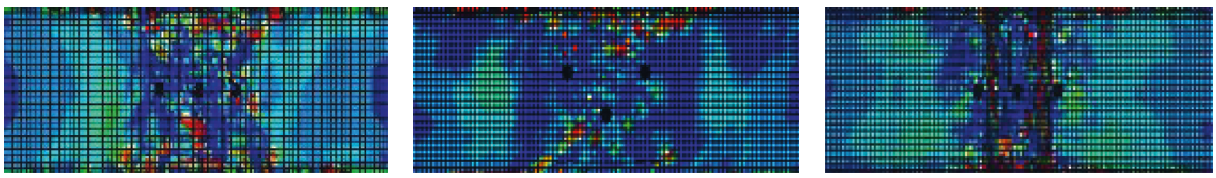

(a) (b) (c)

Figure 14: Mises stress nephogram of roof section in the next 0.3 ms after blasting. (a) "Straight-line" blasting layout. (b) "Triangle-fractal" blasting layout. (c) "Deep-shallow-fractal" blasting layout.

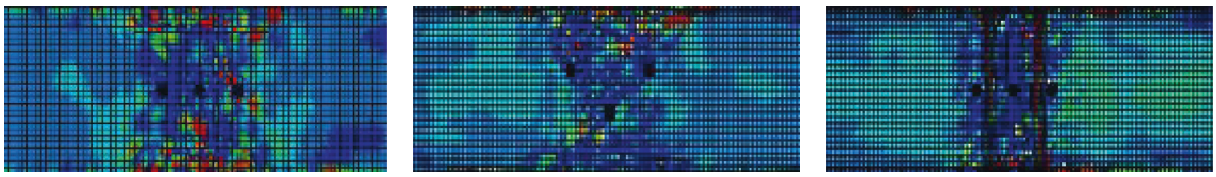

(a) (b) (c)

Figure 15: Mises stress nephogram of roof section in the next 0.45 ms after blasting. (a) "Straight-line" blasting layout. (b) "Triangle-fractal" blasting layout. (c) "Deep-shallow-fractal" blasting layout.

distances from the left side of the hole of 1 m, 3 m, and 5 m, respectively. The differences in the stress peaks at the monitoring points were not obvious. The stress peaks of the three types of placement schemes at #1 monitoring points were all approaching 38 MPa. The peak values of the three kinds of blasting layout schemes in the #2 monitoring points were all close to 32 MPa and at the #3 monitoring points were all close to 28 MPa. These results indicated that the closer the hole was to the monitoring point, the greater the peak value of the stress would be. The peak stress of the three monitoring points was found to be less than the tensile strength of the rock mass, which indicated that the diameter of the broken zone of the rock mass was less than 1 m. Also, the formation of the cracked area and the penetration of the fractures between the adjacent holes required a greater reflection of the tensile stress wave.

It was observed that after the first peak of the stress wave, the stress wave of the "straight-line" blasting layout decayed rapidly and tended to finally approach a zero value. Meanwhile, for the other two schemes, when their stress wave values attenuated to half of their peak value, a stress rebound phenomenon occurs. Then, their stress wave gradually decayed once again and eventually reached a zero value. In the middle and late stages of the blasting process, the equivalent stress of the three schemes was constantly oscillating, and stress rebound phenomena occurred. The stress rebound phenomena of the "deep-shallow-fractal" blasting layout was the most conspicuous, followed by the "triangle-fractal" blasting layout. However, the phenomena of the stress rebound of the "straight-line" blasting layout were not obvious. These findings indicated that the stress wave of the blasting layouts with high fractal dimensions would be continuously reflected in the rock fractures and thereby have sustained effects on the rock mass instead of spreading toward the far end. This would contribute to the desired expansion of the crack zone and the formations of penetrating cracks between the adjacent blast holes.

In this study, by combining the Mises stress nephogram and the equivalent stress nephogram of the monitoring point, it was found that the larger the fractal dimension of the blasting layout was, the larger the stress concentration zone of the blasting stress wave would be, and the longer the duration would be. This would also result in more obvious monitoring point stress rebound phenomena. Therefore, the fractal blasting layout could potentially improve the fractal dimensions of the blasting, as well as increase the crack zone, and enhance the possibility of crack extenuations in multiple directions. Furthermore, the increases in the fractal dimensions of the blasting layout could result in increasingly complex initial cracks, which would have reflective and tensile effects similar to the free surfaces, and cause the cracks to expand further. After the crack expansion, the blasting gas would enter the initial fractures and further expand them. In this way, the new complex fractures would have the continuous oscillating tensile action of the stress waves. This would prevent the stress waves from diffusing outward and result in the energy fully acting within the fractures, thereby prolonging the effects of the stress waves.

5.3.2. Simulation Analysis of Blasting Strain Area. It is known that strain will occur when blasting actions affect rock masses, and the rock masses become damaged as the strain reaches its limit. In order to compare the blast effects of the different blasting layouts examined in this study, the magnitudes of the strain values around the blast holes (warm tone depth) and the geometric characteristics of the observed effective strain regions were also taken into consideration.

The effect dimensions of the "triangle-fractal" and "deep-shallow-fractal" blasting layouts were a vertical-hole surface and a parallel-hole surface, respectively. In order to intuitively compare the effects of the different blasting layout schemes on strain regions, the two types of fractal blasting

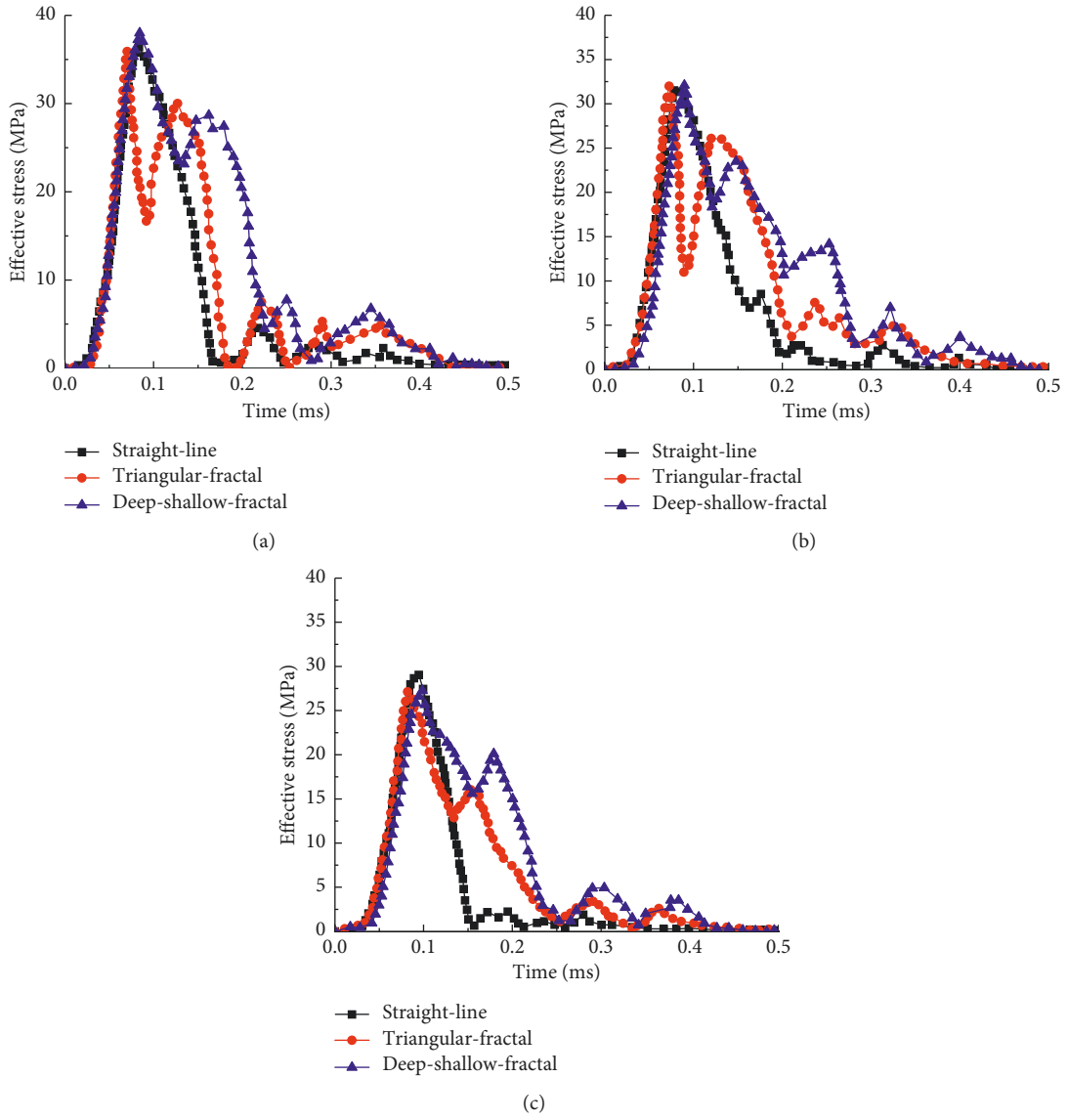

Figure 16: Variation of monitoring points of the Mises stress. (a) Monitoring point 1. (b) Monitoring point 2. (c) Monitoring point 3.

layout schemes were compared with the traditional "straight-line" blasting scheme. It was observed that the "straight-line" and "triangle-fractal" blasting layouts could be compared by the angle of the vertical-hole section (Figure 17(a)). The "straight-line" blasting layout and "deep-shallow-fractal" blasting layout could be compared with the angle of the parallel-hole section (Figure 17(b)).

The strain ranges of the three schemes were found to gradually increase with the blasting times, and the strain value in the area between adjacent blastings holes also gradually increased (warm tone region). In this study, by comparing the strain regions of the "straight-line" and "triangle-fractal" blasting layouts, it could be seen that there was a high strain region in the "triangle-fractal" characterized by a zigzag-shape line. Meanwhile, the high-strain region of the "straight-line" layout was a line shape. In addition, the "triangle-fractal" arrangement displayed large strains in the middle of two distant holes. These results indicated that the fracture bifurcation displayed by the "triangular-fractal" scheme was more likely to be beneficial to the crack propagation. It was also found that the effective strain range of the "triangle-fractal" blasting layout was larger than that of the "straight-line" blasting layout, and the blasting effects were superior.

In this study's comparison of the "deep-shallow-fractal" and "straight-line" blasting layouts, it was found that the high-strain region formed by the "deep-shallow-fractal" blasting layout was also in a zigzag-shape line. A larger strain region had also been formed between two distant points in the "deep-shallow-fractal" blasting layout. These findings indicated that the "deep-shallow-fractal " blasting layout had better energy utilization effects and that the stress waves and exploding gases had acted more fully on the rock mass.

In accordance with the simulation results of the stress and strain, it was found that the larger the fractal dimension was, the slower the attenuation speed of the stress wave would be,

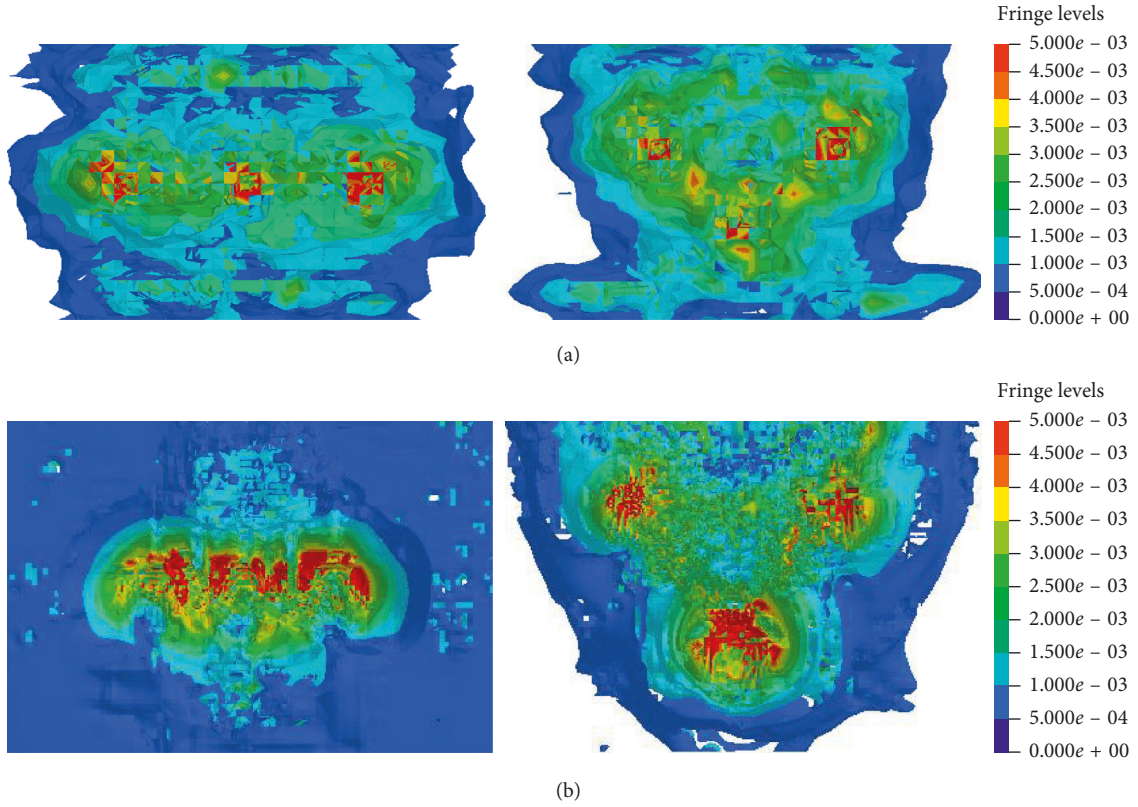

Figure 17: Comparison of max principal strain. (a) Comparison of "straight-line" blasting layout and "triangle-fractal" blasting layout. (b) Comparison of "straight-line" blasting layout and "deep-shallow-fractal" blasting layout.

and the more obvious the changes in the strain values would be. This was observed to be helpful in the breakage of the rock mass and the penetrations of the resulting fractures. Therefore, the entire weakening effects of the blasting on the coal mine's roof areas could be effectively improved.

6. Conclusions

(1) The mechanism of the deep-hole roof blasting and crushing in the Bayangaole Coal Mine were analyzed in this study. The effectiveness range of the explosives was theoretically analyzed, and the reasonable distance between the adjacent holes was determined to be about 10 m.

(2) While conducting an optimization analysis of the layout of the blasting holes based on a fractal theory, this study proposed two optimization blasting layouts: "deep-shallow-fractal" and "triangle-fractal" blasting layouts. The results showed that the fractal dimensions of the traditional "straight-line," "triangle-fractal," and "deep-shallow-fractal" blasting layouts were 1.0, 1.274, and 1.556, respectively. It was determined that the larger the fractal dimensions were, the more the cracking bifurcation opportunities would be created, which resulted in increased quantities of fractures, as well as higher complexity in the fracture areas.

(3) In this study, LS-DYNA software was used to simulate the laws of the stress and strain evolutions in the three blasting layout schemes. The results showed that the "deep-shallow-fractal" blasting layout had the most effective blasting effects, followed by the "triangle-fractal" blasting layout. However, the "straight-line" blasting layout was found to have the least effective performance in the simulation. Also, the simulation results verified that, from the perspective of the stress and strain values, the larger the value of the fractal dimension was, the higher the blast energy utilization rate would be, and the more effective the roof-blasting process would be.

Data Availability

The figures and tables data used to support the findings of this study are included within the article.

Conflicts of Interest

The authors declare that they have no conflicts of interest.

Acknowledgments

The authors gratefully acknowledge the support from the National Natural Science Foundation of China (51622404 and 11572343), the Yueqi Outstanding Scholar Award

Program by CUMTB, the State Key Research Development Program of China (2016YFC0801404), and the Outstanding Young Talents of "Ten Thousand People Plan."

References

[1] J. Drzewiecki and J. Kabiesz, "Dynamic events in roof strata-occurrence and prevention," *Coal Science and Technology Magazine*, vol. 1, no. 1, pp. 55–57, 2008.

[2] Y. M. Lekontsev and P. V. Sazhin, "Directional hydraulic fracturing in difficult caving roof control and coal degassing," *Journal of Mining Science*, vol. 50, no. 5, pp. 914–917, 2015.

[3] J. Maiti, V. V. Khanzode, and P. K. Ray, "Severity analysis of Indian coal mine accidents - a retrospective study for 100 years," *Safety Science*, vol. 47, no. 7, pp. 1033–1042, 2009.

[4] J. Maiti and V. V. Khanzode, "Development of a relative risk model for roof and side fall fatal accidents in underground coal mines in India," *Safety Science*, vol. 47, no. 8, pp. 1068–1076, 2009.

[5] O. I. Chernov, "Hydrodynamic stratification of petrologically uniform strong rocks as a means of controlling intransigent roofs," *Soviet Mining Science*, vol. 18, no. 2, pp. 102–107, 1982.

[6] J.-S. Moon, "Representativeness of jointed rock mass hydraulic conductivity obtained from packer tests for tunnel inflow rate estimate," *International Journal of Rock Mechanics and Mining Sciences*, vol. 48, no. 5, pp. 836–844, 2011.

[7] K. Matsui, H. Shimada, and H. Z. Anwar, "Acceleration of massive roof caving in a long wall gob using a hydraulic fracturing," in *Proceedings of the 99th International Symposium on Mining Science and Technology*, pp. 43–46, Beijing, China, August 1999.

[8] P. Konicek, K. Soucek, L. Stas, and R. Singh, "Long-hole destress blasting for rockburst control during deep underground coal mining," *International Journal of Rock Mechanics and Mining Sciences*, vol. 61, pp. 141–153, 2013.

[9] C. Sawmliana and P. Pal Roy, "A new blastability index for hard roof management in blasting gallery method," *Geotechnical and Geological Engineering*, vol. 30, no. 6, pp. 1357–1367, 2012.

[10] A. S. Paine and C. P. Please, "An improved model of fracture propagation by gas during rock blasting-some analytical results," *International Journal of Rock Mechanics and Mining Sciences & Geomechanics Abstracts*, vol. 31, no. 6, pp. 699–706, 1994.

[11] H. Xie, J. Wang, Z. Chen et al., "Study on top coal blasting technique of full mechanized caving in the hard thick coal seam," *Journal of China Coal Society*, vol. 24, no. 4, pp. 350–354, 1999.

[12] H. Xie, Z. Chen, F. Duan et al., "Fractal study on blasting energy of top coal," *Mechanics and Engineering*, vol. 22, no. 1, pp. 16–18, 2000.

[13] H. Xie, "Fractal geometry and its application to rock and soil materials," *Chinese Jounal of Geotechnical Engineering*, vol. 14, no. 1, pp. 14–24, 1992.

[14] J. Song and K. Kim, "Micromechanical modeling of the dynamic fracture process during rock blasting," *International Journal of Rock Mechanics and Mining Sciences & Geomechanics Abstracts*, vol. 33, no. 4, pp. 387–394, 1996.

[15] L. F. Trivino and B. Mohanty, "Assessment of crack initiation and propagation in rock from explosion-induced stress waves and gas expansion by cross-hole seismometry and FEM-DEM method," *International Journal of Rock Mechanics and Mining Sciences*, vol. 77, pp. 287–299, 2015.

[16] W. B. Lu and Z. Y. Tao, "A study of fracture propagation velocity driven by gases of explosion products," *Explosion & Shock Waves*, vol. 14, no. 3, pp. 264–268, 1994.

[17] J. Zuo, Y. Sun, W. Liu et al., "Mechanical analysis and blasting mechanism of main roof initial fracturing in shallow depth mining face with large cutting height," *Journal of China Coal Society*, vol. 41, no. 9, pp. 2165–2172, 2016.

[18] M. M. D. Banadaki and B. Mohanty, "Numerical simulation of stress wave induced fractures in rock," *International Journal of Impact Engineering*, vol. 40, no. 2, pp. 16–25, 2012.

[19] J. Xu and M. Qian, "Method to distinguish key strata in overburden," *Journal of China University of Mining & Technology*, vol. 29, no. 5, pp. 463–467, 2000.

[20] A. Tavallali and A. Vervoort, "Effect of layer orientation on the failure of layered sandstone under Brazilian test conditions," *International Journal of Rock Mechanics and Mining Sciences*, vol. 47, no. 2, pp. 313–322, 2010.

[21] X. Wang and Z. Wang, *Application of Fractal Theory in the Presplitting Blasting Engineering*, China Molybdenum Industry, Luoyang, China, 2004.

[22] X. Wang, Z. Wang, and S. Feng, "Fracture principle in the prespliting blasting," *Explosion & Shock Waves*, vol. 1, pp. 54–60, 1983.

[23] D. L. Birkimer, "Possible fracture criterion for the dynamic tensile strength of rock," *Stellenbosch Stellenbosch University*, vol. 110, no. 464, pp. 427–441, 1970.

[24] J. Dai, "Calculation of radii of the broken and cracked areas in rock by a long charge explosion," *Journal of Liaoning Technical University*, vol. 20, no. 2, pp. 144–147, 2001.

[25] H. Xie and F. Gao, "The fractal features of the damage evolution of rock materials," *Chinese Journal of Rock Mechanics & Engineering*, vol. 10, no. 1, pp. 74–82, 1991.

[26] C. Mortensen and P. C. Souers, "Optimizing code calibration of the JWL explosive equation-of-state to the cylinder test," *Propellants Explosives Pyrotechnics*, vol. 42, no. 6, pp. 616–622, 2017.